Journal of the European Ceramic Society 40 (2020) 1557–1565

Contents lists available at ScienceDirect

Journal of the European Ceramic Society

journal homepage: www.elsevier.com/locate/jeurceramsoc

Improved crack resistance and thermal conductivity of cubic zirconia containing graphene nanoplatelets

A. Gómez-Gómez[a], C. Ramírez[a], J. Llorente[a], A. Garcia[b], P. Moreno[b], H. Reveron[c], J. Chevalier[c], M.I. Osendi[a], M. Belmonte[a], P. Miranzo[a,*]

[a] Instituto de Cerámica y Vidrio (ICV-CSIC), C/ Kelsen 5, 28049, Madrid, Spain
[b] Grupo de Investigación en Aplicaciones del Láser y Fotónica (ALF-USAL), Universidad de Salamanca, Plaza de la Merced s/n, 37008, Salamanca, Spain
[c] Université de Lyon, INSA-Lyon, MATEIS UMR CNRS 5510, 7 Avenue Jean Capelle, 69621, Villeurbanne Cedex, France

ARTICLE INFO

Keywords:
Zirconia
Graphene nanoplatelets
Composites
R-curve
Thermal conductivity

ABSTRACT

Composites of 8 mol.% yttria-stabilized zirconia (8YSZ) with graphene nanoplatelets (GNP) have been pointed as alternative interconnectors in SOFC due to their mixed ionic-electronic conduction. Here we show that GNP addition provides rising crack-resistance behavior, with long crack toughness up to 78% higher than that of 8YSZ, also improving its thermal conductivity (up to 6 times for the in-plane direction). Toughness versus crack length is measured for 7 and 11 vol.% of GNP using single edge V-notched beam technique and ultrashort pulsed laser notching; and thermal behavior is analyzed by the laser flash method. Materials also have highly anisotropic coefficient of thermal expansion. These properties contribute to enhance their performance under the harsh operating conditions of SOFC, as thermal residual stresses could be reduced while significantly improving the system mechanical stability. Moreover, the heat transfer may be enhanced especially along the interface direction which would increase the system efficiency.

1. Introduction

The ability of graphene for tailoring composite properties using very low filler contents is one of its main advantages in the design of textured composites, multilayers, coatings, 3D printed structures and bioinspired materials. For instance, the electrical conductivity (σ_e) of ceramics can be increased by several orders of magnitude using dispersed platelets, either of graphene (GNP) or reduced graphene oxide (rGO), above their respective percolation thresholds [1]. Two recent works on 8 mol% yttria-stabilized cubic zirconia (8YSZ) ceramics, the most widely used solid electrolyte, claim that 8YSZ/GNP bulk composites are ideal candidates for high-temperature electrochemical devices [2,3], in particular, as interconnects in solid oxide fuel cells (SOFC). Interconnect physically separates and electrically connects the anode of one cell to the cathode of the neighbor, therefore, it should exhibit proper electrical and thermal performances as well as good mechanical integrity. Significant increases of σ_e at 300 °C, from $\sim 4 \times 10^{-4}$ S·m^{-1} of 8YSZ to values up to ~ 10 S·m^{-1}, were reported by Marihna and Belmonte for GNP contents of ~11–14 vol.% [2]. In addition, these authors evidenced the high stability of 8YSZ/GNP composites, showing almost time-independent σ_e values and non-significant material degradation at the demanding conditions of temperature and oxygen partial pressure (P_{O2}) typically required for interconnect materials (P_{O2} from 10^{-4} to $10^{-0.7}$ atm on the cathode side and from 10^{-18} to 10^{-8} atm in the anode side, and operating temperatures of ~800 °C) [4].

The addition of GNP to 8YSZ may increase the very low thermal conductivity of 8YSZ (~2 W·m^{-1} K^{-1}) [5] as well, as it has been already proved for other ceramic matrices [1]. If the thermal conductivity is improved, the efficiency of engineering processes where heat transfer takes place would augment; in particular, for SOFC, it would favor the transport of heat generated at the cathode to the anode, where it can be utilized for the endothermic fuel reforming reaction [4]. Additionally, the use of 8YSZ/GNP composites would limit the mismatch between the coefficients of thermal expansion (CTE) of the different SOFC components, specifically, the 8YSZ solid electrolyte and Ni/8YSZ anode, both with high CTE values (10.5 and 11–12 $\times$ 10^{-6} K^{-1}, respectively [6,7]). Hence, the development of thermal stresses would be reduced during the critical startup and shutdown operations of the SOFC stack. As the risk of crack propagation due to mechanical or thermal stresses is critical for interconnects acting as a structural support, the expected toughening of brittle 8YSZ ceramics (toughness below 1.5 MPa m$^{1/2}$) [8] by the GNP addition [1,9,10] becomes of fundamental interest for the overall SOFC performance.

Toughness improvement has been claimed in ceramic/graphene

* Corresponding author.
E-mail address: pmiranzo@icv.csic.es (P. Miranzo).

https://doi.org/10.1016/j.jeurceramsoc.2019.12.016
Received 1 November 2019; Received in revised form 5 December 2019; Accepted 6 December 2019
Available online 11 December 2019
0955-2219/ © 2019 Elsevier Ltd. All rights reserved.

composites through crack-bridging mechanisms that combine stretching, debonding, sliding and pull-out of the internal graphene layers [9,10]. Based on this evidence, crack growth resistance is expected to increase with crack extension (rising R-curve behavior) in these composites. Although the usefulness of R-curves for predicting the behavior of naturally occurring flaws is evident, only few works deal to this matter in the case of ceramic/GNP composites [11,12] mainly due, on one hand, to the inherent problems of making reliable, reproducible and sharp notches in brittle materials, such as 8YSZ; and, on the other hand, to complications associated with the consistency of toughness values owing to the variability of graphene nanostructures size, degree of exfoliation, degree of functionalization, and quality of graphene dispersion.

One accomplishment of this work was to demonstrate that the rising R-curve behavior of ceramic/GNP composites could be measured by single edge V-notched beam (SEVNB) technique and using ultrashort pulsed laser notching to produce smooth reproducible notches with expected limited thermal damage on the surrounding material. Notching is based on ultrafast laser ablation. The laser light is absorbed by means of non-linear mechanisms within a thin layer of the surface providing almost complete ionization and subsequent ejection of the material by coulomb and/or phase explosion in time scales that preclude significant thermal coupling with the crystalline lattice out of the ablated zone. This notching method has been assessed recently in few quite tough ceramics (alumina [13] and tetragonal zirconia polycrystals doped with 3 mol.% yttria, 3YTZP [14]) but never used for so brittle 8YSZ-based materials. Considering the preferential orientation of the GNP with the ab-plane perpendicular to the SPS loading axis, the R-curve behavior of 8YSZ/GNP composites is analyzed in two different orientations, i.e., the crack paths perpendicular and parallel to the SPS axis. The thermal properties, coefficient of expansion, diffusivity (α) and conductivity (κ), are also studied as a function of the temperature for increasing additions (0–20.7 vol.%) of GNP in the perpendicular and parallel orientations to analyze the previously mentioned enhanced performance of 8YSZ/GNP composites.

2. Experimental part

8YSZ powders of ~ 90 nm (TZ-8YS, Tosoh Co., Japan) and GNP (N006, Angstron Materials Inc., USA) with nominal thickness of 10–20 nm and ~14 μm of lateral dimensions were used as raw materials. 8YSZ/GNP composites containing up to 20.7 vol.% of GNP were prepared following the procedure described in a previous paper [2], which basically consisted in the homogenous mixing of two separately dispersed suspensions in isopropyl alcohol media of GNP (sonicated for 1 h in an ultrasonic bath) and 8YSZ powders (attrition milled for 30 min) in the established proportions. After solvent evaporation, the 8YSZ/GNP powder mixtures were spark plasma sintered (SPS, SPS-510CE, Fuji Electronic Industrial Co., Ltd., Japan) in a vacuum atmosphere of 6 Pa. SPS parameters (temperature, holding time and applied mechanical pressure) were fitted in order to get same densification level for specimens of different GNP contents and dimensions (see Table 1). In this way, thin specimens (2.2 mm) of 20 mm diameter were sintered at 1310 °C (monolithic 8YSZ material) and 1350 °C (8YSZ/GNP composites); whereas, thicker specimens of 30 mm diameter for R-curve tests were sintered at 1320 and 1370 °C, respectively. The specimens were labelled according to the amount of GNP (Table 1) and the testing direction in the case of the R-curve measurements.

8YSZ/GNP composites were > 98.5% dense and showed homogenous microstructure formed by cubic 8YSZ equiaxed grains and dispersed GNP preferentially perpendicular oriented to the SPS loading axis in agreement with results by Marihna and Belmonte [2]. The matrix grain size and aspect ratio were similar for all the specimens, independently of the amount of nanoplatelets (1–2 μm of median diameter and 1.4 of aspect ratio). The graphene platelets preserve crystallinity after processing, compared to raw powders, as demonstrated by Raman spectroscopy studies published elsewhere [2] in which the intensity of the D band of graphene, associated to defects, presented a negligible increment.

Table 1
Summary of the tests carried out (α = thermal diffusivity, H = Vickers Hardness, E = Young modulus and R-curve), 8YSZ/GNP compositions used for each one, corresponding label and dimensions, height (h) and diameter (Φ), of the SPS specimens. || (parallel) and ⊥ (perpendicular) symbols indicate the testing orientation in the case of the R-curve tests.

Test	GNP (vol. %)	Label	DISC SIZE	
			h (mm)	Φ (mm)
α / H / E	0	8YSZ	2.2	20
	7.1	8YSZ/7GNP		
	10.5	8YSZ/11GNP		
	13.6	8YSZ/14GNP		
	20.7	8YSZ/21GNP		
R-curve	0	8YSZ	3.5	30
	7.1	8YSZ/7GNP⊥	4.5	
		8YSZ/7GNP//	3.5	
	10.5	8YSZ/11GNP⊥	4.5	
		8YSZ/11GNP//	3.5	

The effect of GNP on the fracture toughness was analyzed by controlled crack propagation curves (R-curve) in 8YSZ/7GNP and 8YSZ/11GNP composites and the reference material (8YSZ) as well, using the SEVNB method in prismatic bars of 25 × 4.0 × 3.0 mm^3, which were machined from SPS discs of 30 mm in diameter and 3.5–4.5 mm of thickness (Table 1). This amount of GNP was selected considering previous results for Si_3N_4 and SiC ceramics reinforced with same GNP where the maximum toughness was achieved for GNP contents in the range of 5 to 10 vol.% [15,16].

As GNP were preferentially orientated with the ab-plane perpendicular to the SPS loading axis, this property was measured for the two different orientations with expected higher toughness increments. As shown in the schemes of Fig. 1a, GNP are perpendicularly oriented to the planar crack front in both orientations but facing either the plane or the edges of the platelets for crack propagating in the direction “perpendicular” or “parallel”, respectively (Fig. 1a). The orientation in which a–b plane of the graphene platelets is parallel to crack propagating plane was not considered as pellet with the thickness equal to the length of the required flexural beam would change composite densification rate during SPS. For this orientation, a diminished reinforcing effect is expected due to the weak Van der Waals forces between the graphene layers. In fact, indentations performed on cross-sections of SiC/GNP composites showed that cracks are suppressed in the direction perpendicular to the a–b plane of the GNP whereas they propagated freely in the horizontal direction [16]. One of the 25 × 4.0 mm^2 lateral surfaces of the bars was polished for later observation of crack paths by scanning electron microscopy. The bars were notched on the 25 × 3.0 mm^2 face. An image of the notch used for the tests is shown in Fig. 1b. A pre-notch of 2 mm depth (50% of the specimen height) and 400 μm width was made using a diamond coated metal blade of 0.3 mm width. Afterwards, for reliable R-curve measurements, a thin and sharp notch of around 200 μm depth was produced at the pre-notch tip by ablation with near infrared ultrashort laser pulses (120 fs, 795 nm). The laser system used is a commercial Ti: Sapphire oscillator (Tsunami, Spectra Physics, USA) and a regenerative amplifier system (Spitfire, Spectra Physics, USA) based on chirped pulsed amplification (CPA). It delivers linearly polarized pulses with a repetition rate of 1 kHz. The pulse energy used was 34 μJ. To attain the energy density on the material surface to unleash ablation, the pulses must be focused with an achromatic doublet lens with focal length 50 mm. The samples were placed on a XYZ motorized stage and moved along one of the horizontal axis with a scanning speed of 125 $\mu m \cdot s^{-1}$. Twenty four passes were needed to achieve the desired notch depth. The notch tip radius with

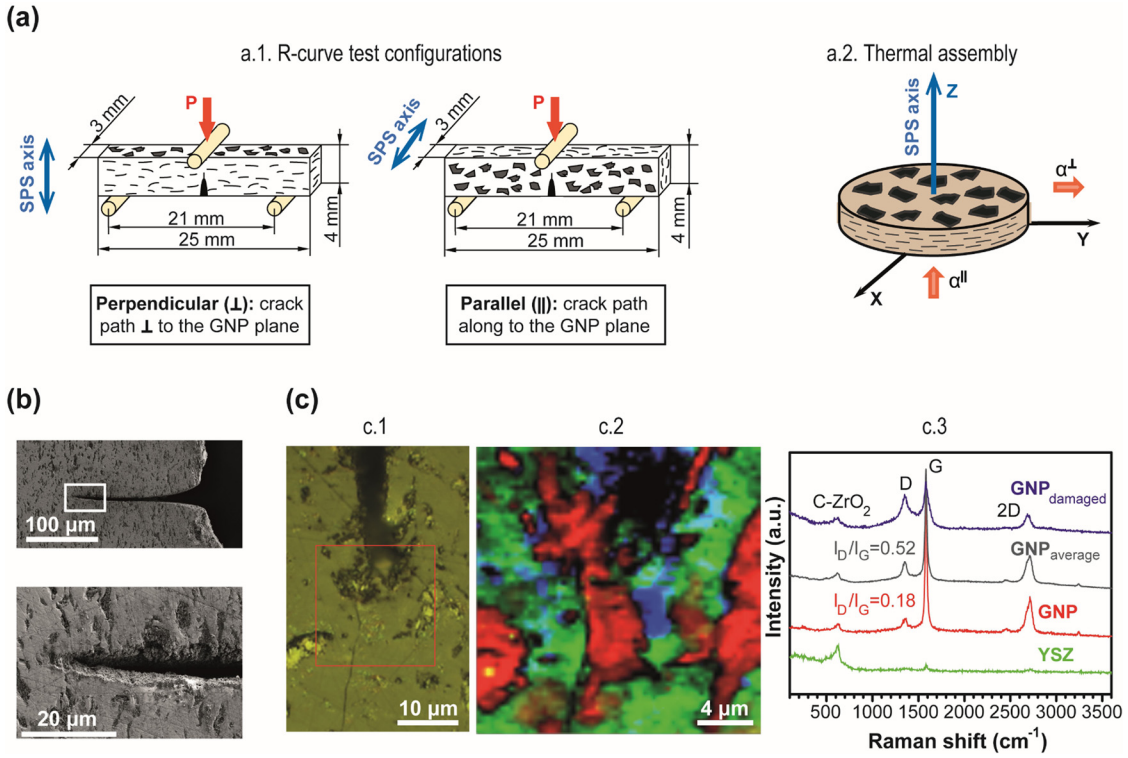

Fig. 1. (a) Schematics of the GNP orientation with respect to (a.1) the crack propagation direction for the two arrangements (perpendicular and parallel) used for the R-curve tests and (a.2) the heat flow for the measurement of thermal diffusivity in the directions perpendicular ($\alpha^{\perp}$) and parallel ($\alpha^{||}$) to the SPS pressing axis. (b) SEM micrographs showing an example of the notches used to attain stable crack propagation that consist of a pre-notch of 400 μm width and a thin sharp notch (radius = 1 μm) produced by ablation with near infrared ultrashort laser pulses. (c) Raman analysis of a notch tip in the 8YSZ/11GNP composite: (c.1) optical image, (c.2) colour-coded image of the area marked in (a) constructed by merging Raman intensity maps of the G-band (1582 cm^{-1}) of GNP, in red, the band of cubic 8YSZ at 630 cm^{-1}, in green, and the ratio of the D and G bands (I_D/I_G), in blue. Representative spectra of each of these areas are included in (c.3) as well as the average of the GNP spectra. Conditions used for Raman spectroscopy: 60 × 60 pixels (one spectrum per pixel and 0.2 s of acquisition time) and laser wavelength excitation of 532 nm (For interpretation of the references to colour in this figure legend, the reader is referred to the web version of this article.).

this procedure is typically of 1 μm (Fig. 2b). Raman spectroscopy (Alpha300 WITec GmbH, Germany) performed on an area of 20 × 20 μm^2 around the tip of the notch in the 8YSZ/11GNP composite (Fig. 1c) confirmed that most of the GNP remained undamaged (Raman intensity ratio between D and G bands of 0.18, similar to the un-notched specimens), and only some GNP degraded by the laser were observed in a small area located less than 5 μm ahead the tip. The notch depth and crack front were observed in several specimens by post fracture analysis; in figure S1 of the supplementary information it can be observed that crack fronts are flat and regular with an approximate notch length of ~ 200 μm.

The notched specimens were tested in 3-point bending, as shown in Fig. 1a, on a Instron 8500+ machine (Norwood, USA) with 21 mm of span; a LVDT positioned close to the notch mouth was used to get a precise record of the specimen displacement. The tests were carried out at two different constant displacement rates, 5 and 10 μm min^{-1}, to evaluate potential slow crack growth effect. The R-curve of 8YSZ/GNP composites was then built from loading-displacements data of controlled crack growth test by the compliance method [17]. The obtained curves were validated estimating the crack length increment by the unloading compliance procedure and physically measuring the crack length at intermediate states by optical (Zeiss, Axiophot, Oberkochen, Germany) and scanning electron (SEM, Tabletop microscope TM-1000, and field emission FESEM, Hitachi, Tokyo, Japan) microscopies. Crack propagation paths (after crack extension during R-Curve tests, before failure) and fresh fracture surfaces were also observed by FESEM.

Instrumented Vickers micro-indentation tests (APEX-1 model, Bruker, USA) were performed at room-temperature on the polished surfaces perpendicular to the SPS axis for all the 8YSZ/GNP specimens, using an indentation load of 1 N. The elastic modulus (E) was obtained from the unloading branch of the load versus penetration depth curves, corrected from the frame compliance of the instrumented indenter. The hardness (H) was calculated from the peak load and the contact area. At least nine indentations were considered on each material, and the mean and standard deviation of data are provided. Despite the anisotropy of ceramic/GNP materials, there are not significant differences in the indentation imprint orthogonal diagonals [1].

The thermal diffusivity of the specimens was measured by the laser-flash method (Thermaflash 2200, Holometrix/Netzsch, USA) in two different directions according to the GNP orientation regarding the SPS pressing axis (Fig. 1a.2). The thermal diffusivity in direction parallel to the SPS pressing axis ($\alpha^{||}$) was measured from room temperature (RT) to 600 °C, in Argon atmosphere, on 8.8 × 8.8 mm^2 square specimens of ~ 0.5–1 mm thickness, machined from discs of 20 mm in diameter (Table 1). Diffusivity for the direction perpendicular to the SPS pressing axis ($\alpha^{\perp}$) was directly measured in disc specimens of 20 mm diameter and ~0.5 mm thickness just at RT, using a special mask in which laser radiation is confined to a small circular area of radius r_0 = 2.5 mm in the center of the sample. In this way, heat flows through the thickness to the rear face and, then, spreads radially, being the emitted infrared radiation detected at an external ring of radius 2.2 times r_0; the temperature rise is then fitted to a two-dimensional model. Reported values are averaged results over, at least, four consecutive measurements. The thermal conductivity (κ) was then calculated from α data using the equation:

$$\kappa = \alpha \cdot \rho \cdot C_P \quad (1)$$

where ρ is the density and C_p the specific heat, which was calculated by the rule of mixtures from the percentage of GNP in the sample and the

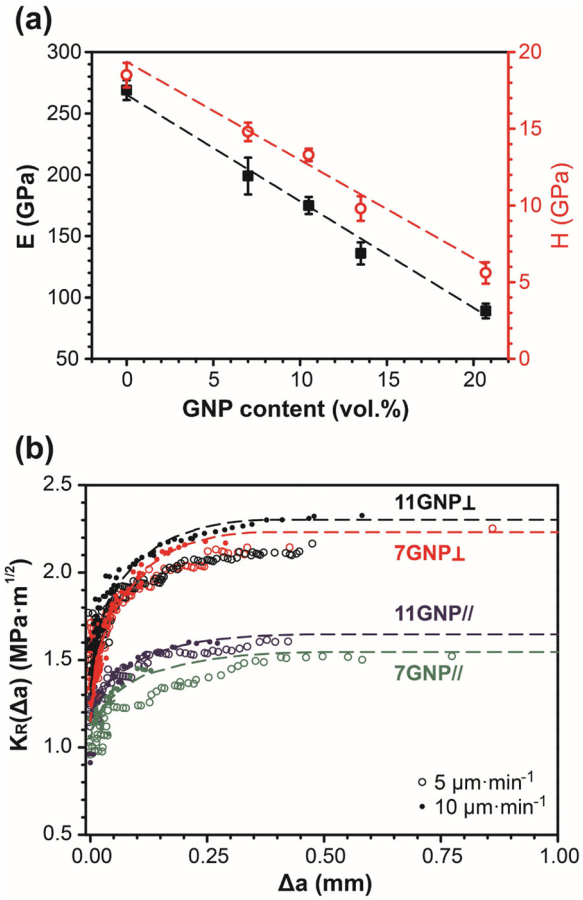

Fig. 2. (a) Elastic modulus (E) and hardness (H) of 8YSZ/GNP composites as a function of the GNP content. (b) Crack resistance (K_R) of 8YSZ/7GNP and 8YSZ/11GNP composites versus crack extension (Δa) measured using SEVNB at various loading rates and for perpendicular (⊥) and parallel (||) orientations. Dashed lines are fittings of the experimental crack growth data to equations for R-curve [24], performed at 10 μm. min^{-1}.

specific heat of graphite and 8YSZ data from literature [18]. Error bars in thermal conductivity plots correspond to the estimated accuracy of the laser flash technique for $\kappa^{||}$ data, ~7%, and the standard deviation of the values for $\kappa^{\perp}$.

For CTE measurements, a differential dilatometer (model Netzsch Netzsch DIL402PC, Germany) provided with a silica sample holder was used on plane-parallel bars of 12 × 3.0 × 4.0 mm^3 size. The CTE was measured in the longer axis of the specimens (i.e. the direction perpendicular to the SPS pressing axis) up to temperatures of 400 °C and using a heating rate of 5 °C min^{-1}. It was also measured in the direction of the SPS axis on smaller specimens of 3 mm length. The anisotropy in CTE was also checked for the 8YSZ/11GNP composite by recording the area and shape factor changes with temperature with an optical dilatometer (Hot-stage miscroscope Leitz, Germany) at constant heating rate of 10 °C· min^{-1} from RT up to 300 °C in air, using specimens of 3 × 3 x 3 mm^3 machined from the mechanically tested bars. The projected shadow image was recorded as a function of temperature by the CCD camera. Results are included in the supplementary information.

3. Results and discussion

3.1. Mechanical properties

Fig. 2a displays the effect of the GNP content on the hardness and elastic modulus of 8YSZ/GNP composites, obtained by micro-indentation; both parameters significantly diminished with increasing GNP content, from 18.5 to 5.5 GPa (decrease of 69%) and from 269 to 89 GPa (decrease of 67%), respectively, for the 8YSZ/21GNP composite. This softening effect with the GNP content for ceramic/GNP composites [1,19] has already been observed and, in the particular case of Si_3N_4/GNP composites [19], where elastic constants were calculated from resonant ultrasound spectroscopy data, a similar reduction of E (75% for 18 vol.%GNP) has been reported in the direction perpendicular to the GNP plane, whereas E decreased just by 27% along the GNP plane direction. Moreover, E became progressively more anisotropic with the amount of nanoplatelets owing to their preferential orientation and intrinsic anisotropy [19]. The large reduction in E for the perpendicular direction was explained by the low out-of-plane modulus of graphite (36.5 GPa [20]).

The discussion on the reasons for such important reductions is not trivial considering the complex stress distribution developed under the indenter and the anisotropy of the present materials; it is assumable that if the indentation depth is sufficiently large, the measured E values may be representative of the structure as a whole. However, in our case, the simplest approximation of the rule of mixtures that establishes the upper and lower bounds of the elastic modulus revealed that experimental values fit well to the lower bound gave by the Reuss model for isostress condition, providing more weight to the low transverse modulus of GNP (36.5 GPa for graphite [20] and 50 GPa for multilayer graphene as calculated by MD simulation [21]). This is in agreement with a finite element numerical study performed on metal-ceramic multilayered composites showing that the effective modulus obtained by indentation is representative of the out-of-plane modulus of the composite [22].

Regarding hardness, the substantial reduction can be linked to the nucleation of mode II microcracks due to the matrix/graphene interface debonding by a shear faulting process, as it has been proved by Hertzian contact tests in SiC/graphene composites [23]. Accordingly, enlarged quasi-plastic damage response with increasing graphene content was observed for these materials.

GNP additions clearly modified the fracture behavior of the 8YSZ (see examples in Figure S2 of the supplementary information). Whereas it was not possible to reach a controlled crack growth in the case of the monolithic material because the catastrophic fracture of the specimens occurred owing to their quite brittle nature, 8YSZ/GNP specimens showed a nonlinear stress-strain curve with an initial linear-elastic region followed by a non-elastic zone. Fig. 2b shows R-curves at 5 and 10 μm min^{-1} for 8YSZ/7GNP and 8YSZ/11GNP composites in the two tested orientations, as well as the corresponding fittings (dashed lines in the figure) of the experimental crack growth data to equations for R-curve [24]. As seen, lower stress intensity factors are observed for the slower displacement rate, which points to the occurrence of some slow crack growth in the present 8YSZ/GNP composites. This phenomenon is probably associated to corrosion of zirconia matrix by water molecules assisted by stresses at the crack tip, as it is known to occur under static loading in zirconia–based ceramics [25].

Higher crack resistance was achieved for the perpendicular orientation, where the planar crack front is perpendicularly oriented to the GNP a–b plane (Fig. 1a.1). Large effective crack deflection and bridging were clearly perceived for this orientation when observing crack propagation at intermediate states before failure in specimens tested following the unloading compliance procedure (Fig. 3a,b). Conversely, in the parallel direction (Fig. 3c), i.e. crack front facing the platelet edges, almost straight cracks were observed with a less significant contribution of the above reinforcing mechanisms. This behavior also agrees with in-situ crack propagation observations realized on reinforced Si_3N_4/rGO composites, where pull-out and bridging phenomena, among others, were plainly identified [9,10]. The significantly higher reinforcement in the perpendicular orientation would be then linked to a more effective crack-wake bridging by the large and thick GNP stacks, which may stretch thin and split along the weak GNP layers due to the more favorable geometry before their fracture [10].

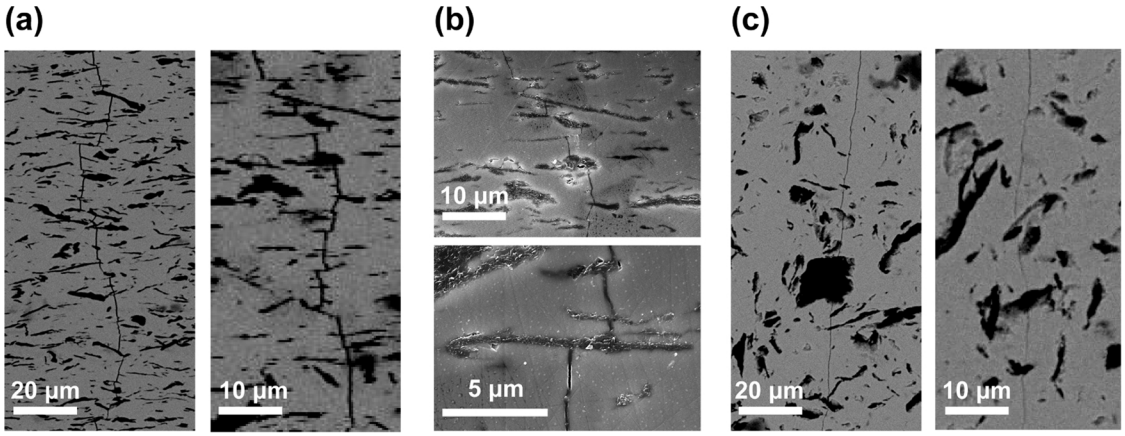

Fig. 3. SEM micrographs showing crack propagation at an intermediate state before failure in the 8YSZ/11GNP composite tested following the unloading compliance procedure: (a) perpendicular arrangement where large effective crack deflection and bridging are clearly perceived, (b) detail showing crack bridging and (c) parallel configuration where crack propagates straight-ahead with an insignificant interaction with GNP.

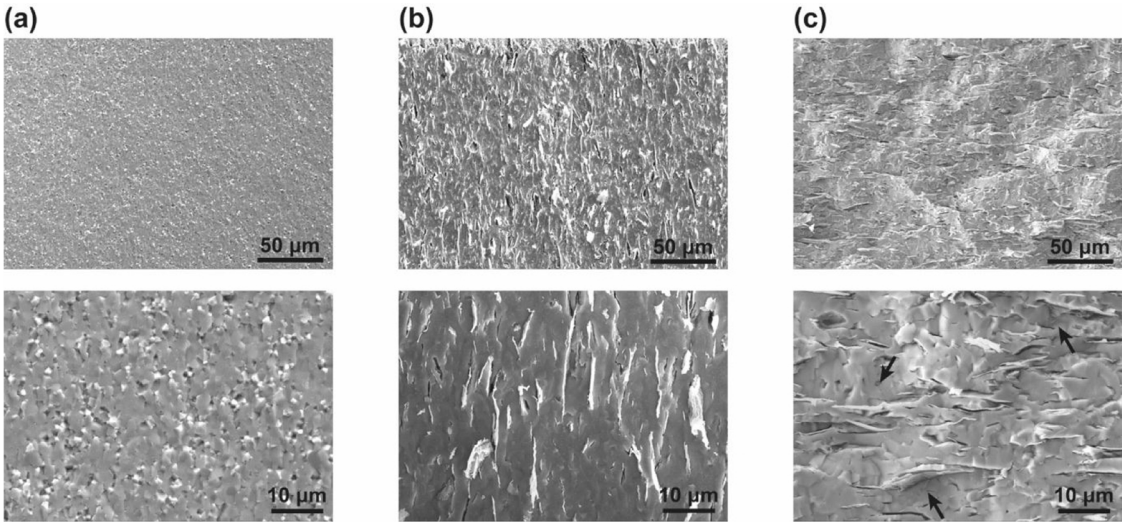

Fig. 4. FESEM micrographs of the fracture surfaces of the reference 8YSZ material (a) and the 8YSZ/11GNP composite for the parallel (b) and the perpendicular (c) mechanical test configurations. Black arrows in (c) indicate areas of crack deflection.

According to these observations, the monolithic 8YSZ reference material mainly showed transgranular smooth fracture surface (Fig. 4a), while numerous pulled-out GNP and important roughness associated to the zirconia matrix (see black arrows in Fig. 4c) were observed on the fracture surfaces of the perpendicularly tested specimens. In the parallel direction (crack front facing the platelet edges), the “effective area” of material intersecting crack front is significantly lower and the contribution of deflection decreased as suggested by the flatness observed in the matrix (Fig. 4b). This anisotropic mechanical behavior can be explained by the development of a complex pattern of residual strains around the nanoplatelets [26].

Fig. 5 includes the present crack growth figures, $K_R(\Delta a)$, for the perpendicular orientation and R-curve data found in the literature for transformation toughened ZrO_2 materials -stabilized using CeO_2, MgO and Y_2O_3- and graphite (adapted from reference [27]), for an Al_2O_3/MWCNT (10 vol.%) composite [28], and for Al2O3 [11] and SiOC glass-ceramic [12] containing graphene fillers (G in Fig. 5). Data were normalized by the initial K_0 value of the R-curves for comparative purposes. The resulting K_R/K_0 values are quite remarkable for the present materials, showing a long-crack resistance value approaching twice the initial toughness, similarly to Mg-PSZ materials. For the rest, K_R/K_0 is below 1.5 with the exception of a SiOC/G composite that showed extraordinary increasing values with crack length, although data for

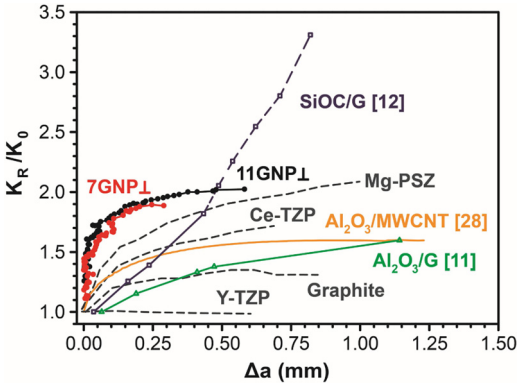

Fig. 5. Comparative of the crack growth $K_R(\Delta a)$ data for the 8YSZ/7GNP and 8YSZ/11GNP in the perpendicular orientation and R-curve data found in the literature for different transformation toughened ZrO_2 materials, graphite, adapted from [27], Al_2O_3/MWCNT [28] and ceramic composites containing graphene fillers (G), from references [11,12]. K_R/K_0 corresponds to the data normalized by the initial value of the R-curves.

Table 2
Parameters obtained from fitting the experimental crack growth data of 8YSZ/11GNP and 8YSZ/7GNP composites to equations for R-curve of a bridged long crack in reference [24]: matrix toughness (K_0), steady state toughness limit (K_∞), bridging stresses (P_m) and crack opening at the limit of bridges disengagements (ξ).

Material	8YSZ/11GNP		8YSZ/7GNP	
nanoplatelet Orientation	⊥	//	⊥	//
K_0 (MPa·m$^{1/2}$)	1.3	1.2	1.2	1.1
K_∞ (MPa·m$^{1/2}$)	2.3	1.6	2.2	1.6
P_m (MPa)	50	24	52	23
ξ (nm)	760	610	640	510

$\Delta a > 0.4$ should be considered with caution as test did not meet with ASTM requirements [12].

Fitting of the experimental crack growth data to equations for R-curve of a bridged long crack and the steady state limit by B. Lawn in reference [24] gave the parameters included in Table 2. K_0 represents the matrix toughness which may be different for different amount of GNP and orientations as it can be affected by the residual stresses. The 8YSZ/11GNP⊥ sample R-curve fitted quite well with K_0 = 1.3 MPa m$^{1/2}$ and a steady state toughness limit (K_∞) of 2.3 MPa m$^{1/2}$, reaching a value of bridging stresses of 50 MPa. These parameters were lower for 8YSZ/11GNP$_{//}$ and the best fit led to K_∞ of 1.6 MPa m$^{1/2}$ and 24 MPa of bridging stresses. The fittings for the 8YSZ/7GNP material, with slightly lower content of GNP, provided lower K_0 (1.2-1.1 MPa m$^{1/2}$ for both orientations) and K_∞ (2.2 and 1.6 MPa m$^{1/2}$ for the perpendicular and parallel orientations, respectively), but similar values for the bridging stresses in both directions. These figures represent increments in the long crack toughness of up to 78%, considering the toughness value of 1.3 MPa m$^{1/2}$ for the monolithic 8YSZ, estimated from the present results and using ASTM C 1421 – 01b standard method. The obtained bridging stresses are of the same order of those (~50 MPa) reported for carbon nanotubes reinforcements (10 vol.% MWCNT) in Al_2O_3 matrix [28], and the crack opening at the limit of bridges disengagements is less than 800 nm for all the cases (ξ in Table 2), slightly lower than to that reported for the Al_2O_3/MWCNT composite (~1 μm). There are certain similarities between GNP and MWCNT that we can reckon as being multilayered materials, the pull-out processes in both nanostructures involve the sliding of more internal parts (layers/tubes) and they share similar theoretical highest value for the elastic modulus. However, a direct comparison between both materials is not straightforward as the influence of microstructural parameters, composition and pre-crack history should be taken into account [29]. In this way, the matrix grain size significantly differs, from ~300 nm of Al_2O_3 [28] to ~1 μm of the present composite, and the same can be said of the dispersing method and their specific geometry (1D or 2D). For the same filler volume, the number of ligaments in the bridged zone is consequently higher for the MWCNT composite, which would explain the slightly higher ξ and more gradual R-curve increment of the Al_2O_3/MWCNT composite, plotted in Fig. 5. On the other hand, the anisotropic CTE of the GNP would play a key role in the lower bridging stresses for the parallel orientation, as it is negative along the ab-plane while it is higher (28 × 10^{-6} K^{-1}) than the 8YSZ matrix (10.5 × 10^{-6} K^{-1}) in the c-axis.

As an analog to fiber failure in composites, the strength of the nanoplatelet (σ_{fGNP}) could be estimated from its elastic modulus and the ratio between the length of unbroken platelet holding the crack and the debonding length [30]. A rough estimation of the platelet strength taking the reported lowest elastic modulus (100 GPa), which corresponds to a highly defective GO [31], and the highest limit for graphene elastic modulus (1 TPa) leads to values in the order of 6 to 60 GPa, considering a debonding length of the same order of the nanoplatelet diameter (14 μm) as observed in in-situ mechanical tests for Si_3N_4/GNP composites [10]. For those composites, σ_{fGNP} of 20 GPa (within the same range) was estimated from the fitting of energy release rate versus filler volume [9].

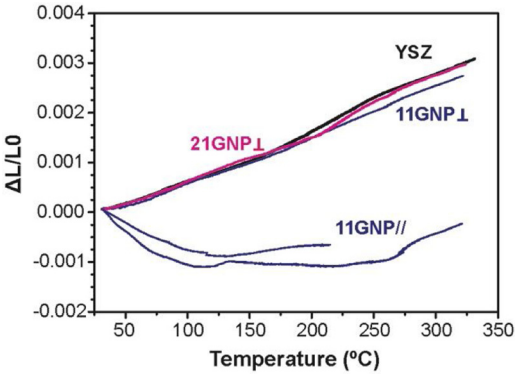

Fig. 6. Dimensional changes as a function of temperature for the reference 8YSZ material and the 8YSZ/11GNP and 8YSZ/21GNP composites in the direction perpendicular to the SPS axis. In the case of the 8YSZ/11GNP, expansion in the parallel direction is also included.

3.2. Thermal properties

As seen in Fig. 6, CTE was not significantly affected by the GNP addition in the direction perpendicular to the SPS axis, i.e. along the platelet ab-plane, where the temperature dependence of the linear expansion is similar for the 8YSZ/11GNP and 8YSZ/21GNP composites and the 8YSZ material (CTE values range from 9.5 to 10.1 × 10^{-6} K^{-1}). Surprisingly, CTE measured in the direction of the SPS axis for the 8YSZ/11GNP composite dropped drastically, becoming negative (-17 × 10^{-6} K^{-1}) up to 100 °C, near zero between 100 and 250 °C and, then, increasing (~ 11 × 10^{-6} K^{-1}) for higher temperatures. Therefore, the CTE of the composite in this direction significantly differs from the average thermal expansion of both components as CTE of 8YSZ matrix and GNP in the c-axis are significantly higher (~ 10 and 28 × 10^{-6} K^{-1}, respectively). This high anisotropy in the CTE was also checked by recording the area and shape factor changes with temperature with an optical dilatometer (results are included in the supplementary information, in Figure S3). A similar strong anisotropy in the CTE has also been reported for copper composites containing highly aligned GNP [32,33], response that authors linked to the residual thermal strains introduced during SPS consolidation, which would lead to larger reduction of elastic constants and Poisson ratio along the SPS direction than in the perpendicular plane where the platelets are preferentially orientated. As it was mentioned before, this anisotropy in the elastic constants has been probed for Si_3N_4/GNP composites by means of resonant ultrasound spectroscopy [19]. The occurrence of residual strains in the present composites was verified by X-ray diffraction (XRD) procedures as presented in Figure S4 of the supplementary information. As seen, the main XRD (111) peak of 8YSZ is shifted to higher angles in the bulk composites compared to the monolithic material, but this shift is insignificant for the corresponding ground samples. This means that the matrix is under average compression in the composites; whereas the GNP filler is under tension.

It should be highlighted that CTE values for the in-plane orientation are close to the reported CTE for the 8YSZ electrolyte and Ni/8YSZ cermet anode, which vary from 10.5 to 12 × 10^{-6} K^{-1}. Therefore, the use of 8YSZ/GNP composites as interconnects in SOFC would allow matching CTE between the different components in the in-plane orientation, while significantly reducing thermal expansion in the direction perpendicular to the interface. Accordingly, the residual stresses in the cell would be reduced and the mechanical stability of systems would be improved.

Thermal conductivity in the parallel direction for the monolithic 8YSZ shows (Fig. 7a) a modest increase with temperature, from 1.9 at

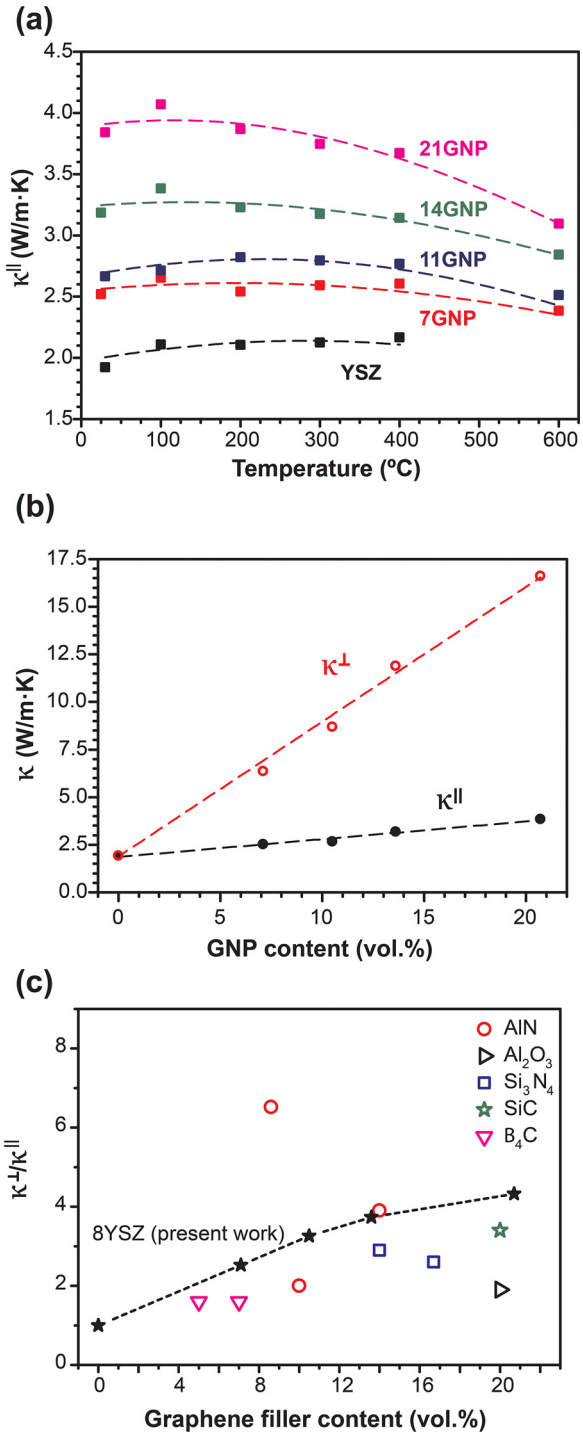

Fig. 7. Thermal conductivity of 8YSZ/GNP composites: (a) as a function of temperature in the parallel direction ($\kappa^{||}$), (b) $\kappa^{||}$ and $\kappa^{\perp}$ and (c) $\kappa^{\perp}/\kappa^{||}$ ratio as a function of the GNP content. For comparative purposes, $\kappa^{\perp}/\kappa^{||}$ data for different ceramic/graphene composites, as reported in reference [1], have been included in (c).

25 °C to 2.1 $W{\cdot}m^{-1}\,K^{-1}$ at 400 °C. The observed downturn in the $\kappa^{||}$ curve for temperatures below 100 °C ($\kappa^{||}_{RT}/\kappa^{||}_{100}$ = 0.91) has theoretically been predicted for 8YSZ ceramics and it was assigned to the additional phonon-scattering due to the oxygen-vacancy hopping between neighboring sites in the 8YSZ lattice [5]. As seen in Fig. 7a–b, $\kappa^{||}$ values increased with the amount of GNP added to the 8YSZ ceramics up to 3.84 $W{\cdot}m^{-1}\,K^{-1}$ (at RT) for 20.7 vol.% of GNP, and their temperature dependence became progressively stronger. However, the reduced $\kappa^{||}$ at

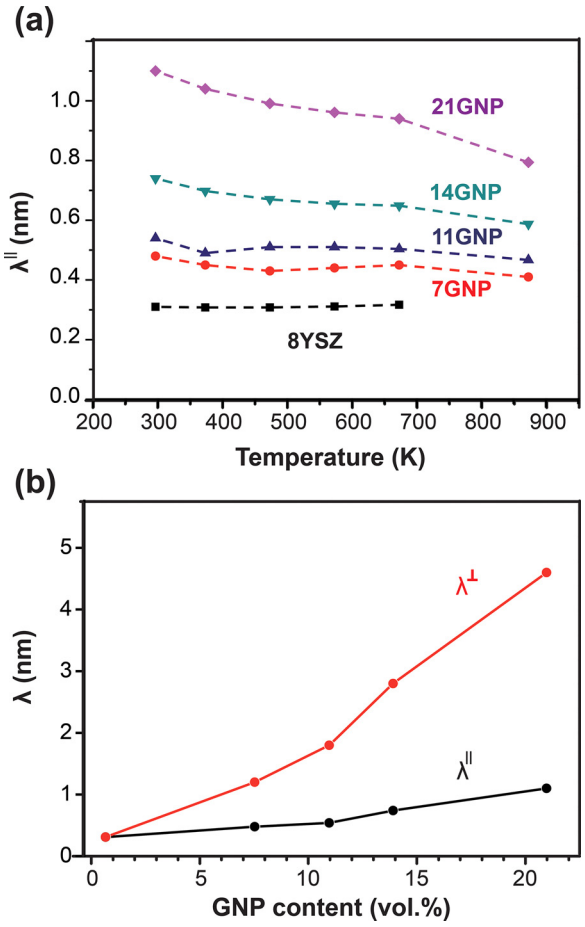

Fig. 8. Phonon mean free path (λ) estimated for 8YSZ/GNP composites as a function of: (a) temperature in the parallel orientation and (b) GNP content for heat flowing parallel and perpendicularly to the SPS axis, at 25 °C.

RT is still detected in all composites, which infers that thermal conduction in this direction is dominated by the 8YSZ matrix. The observed increase in $\kappa^{||}$ was 81%, in contrast to the strong decrease in $\kappa^{||}$ (up to 60%) reported for other ceramic/GNP composites [1]. For the perpendicular orientation where heat flows mainly along the GNP ab-plane, $\kappa^{\perp}$ linearly augmented with the amount of GNP (Fig. 7b), up to 17 $W{\cdot}m^{-1}\,K^{-1}$ for 20.7 vol.% GNP, which is huge (575%) compared to the increments reported for other ceramic matrices that are below 100% [1]. The anisotropy in thermal conductivity (Fig. 7c), defined by the $\kappa\perp/\kappa||$ ratio (up to 4.2), agreed quite well with the general trend observed for ceramic/GNP composites. This anisotropic enhanced thermal conductivity can improve the efficiency of engineering processes where heat transfer in specific directions is required.

According to the kinetic theory of gases [34], the phonon mean free path, λ, can be estimated from the thermal conductivity, the heat capacity per unit volume and the group velocity of acoustic phonons (ν), which can be calculated from the elastic modulus and density of the materials ($\nu = E^{1/2}\rho^{-1/2}$). The $\lambda^{||}$ data deduced for 8YSZ/GNP composites are plotted in Fig. 8a as a function of temperature. As seen, a very constant low value of $\lambda^{||}$ (~0.3 nm) was obtained for the reference 8YSZ, which is linked to the high concentration of oxygen vacancies in this material; effective λ can be considered as an inverse sum of the mean free paths associated to the different phonon scattering interactions, in this case mainly phonon–phonon (p-p), phonon-oxygen vacancies (p-v) and the already mentioned additional phonon scattering due to the oxygen-vacancy hopping between neighboring sites in the 8YSZ lattice (p-vH) [5].

Fig. 8b shows that $\lambda^{||}$ slightly increased with the GNP content, up to

~1.1 nm for 20.7 vol.% GNP, conversely to the trend reported for SiC/GNP composites [35]; for those composites, $\lambda^{||}$ did not depend on GNP content as thermal conduction is dominated by the matrix in this orientation. Besides, temperature dependence of $\lambda^{||}$ became progressively stronger with GNP content (Fig. 8a). This behavior infers a reduction in phonon-scattering in the case of 8YSZ matrix, mainly at low temperatures, due to the presence of GNP, probably linked to a lower contribution of p-vH interactions associated to electrons transfer from GNP to the doubly charged oxygen vacancies in 8YSZ, which would diminish the oxygen-vacancy hopping process. In fact, the high level of hole-doping on graphene has been proved for 8YSZ/graphene composites compared to other oxide matrices such as Al_2O_3 or 3YTZP [36].

Although elastic modulus is expected to be higher in the perpendicular direction [19], we can do a rough estimation of $\lambda^{\perp}$ using the same group velocity, giving values (Fig. 8b) that increased from 0.3 (8YSZ) to 4.6 nm (8YSZ/21GNP), in a similar way to the trend observed for SiC/GNP composites [35].

Reported thermal conductivity data for ceramic/GNP composites offer a very reasonable fitting to a simple model of thermal resistors using GNP thermal conductivity values of 152 $W{\cdot}m^{-1}\,K^{-1}$ and 4.5–9.9 $W{\cdot}m^{-1}\,K^{-1}$, for in-plane and through-thickness directions, respectively [1]. The fit of this model to present $\kappa^{\perp}$ data (8YSZ/GNP composites) gives a considerably reduced thermal conductivity (66 $W{\cdot}m^{-1}\,K^{-1}$) for similar GNP ; whereas, for $\kappa^{||}$ data, increasing κ values for the 8YSZ matrix (from 1.9 up to 3.4 $W{\cdot}m^{-1}\,K^{-1}$ for 20.7 vol.% GNP) was deduced from the fitting. The reduced κ for GNP and increased κ for 8YSZ would be in agreement with the proposed hole-doping of GNP and reduced oxygen vacancy hopping in the 8YSZ matrix, respectively.

4. Conclusions

8YSZ/GNP composites show strongly rising R-curve behavior with improved long crack toughness (78% improvement for 11 vol.% GNP) for cracks facing the GNP planes due to the occurrence of crack deflection and bridging mechanisms. These materials are highly tolerant owing to the improved toughness and reduced elastic modulus.

Unexpectedly, the CTE significantly differs from the average thermal expansion of the two composite components; it is similar to that of the 8YSZ ceramics in the plane where GNP are mainly oriented, while it considerably drops in the perpendicular direction, which would allow CTE matching between the different components to reduce residual thermal strains.

Thermal conductivity is significantly enhanced in both through-thickness and in-plane orientations, maintaining the high anisotropy in the thermal performance of ceramic/GNP composites fabricated by SPS. Charge transfer between graphene and 8YSZ explains the deviations from the behavior observed for other ceramic/graphene composites.

All these properties would contribute to enhance the performance under harsh operating conditions, considerably improving the system mechanical stability, as well as the efficiency of engineering processes where heat transfer in specific directions is required.

Accordingly, additions of well dispersed GNP to 8YSZ ceramics allow developing composites with very peculiar mechanical and thermal properties that may significantly extend its field of application

Declaration of Competing Interest

The authors declare that they have no known competing financial interests or personal relationships that could have appeared to influence the work reported in this paper.

Acknowledgements

This work was supported by Spanish project RTI2018-095052-B-I00, Ministerio de Ciencia, Innovacion y Universidades, Spain (MCIU/AEI/FEDER, UE). AG and PM acknowledge support from Ministerio de Economía, Industria y Competitividad, Spanish government (Project FIS2017- 87970-R) and Junta de Castilla y León, Spain (Project SA287P18). C. R. thanks the financial support by MCIU under contract IJCI-2017-34724 of “Juan de la Cierva” Program.

Appendix A. Supplementary data

Supplementary data associated with this article can be found, in the online version, at https://doi.org/10.1016/j.jeurceramsoc.2019.12.016.

References

[1] P. Miranzo, M. Belmonte, M.I. Osendi, From bulk to cellular structures: a review on ceramic/graphene filler composites, J. Eur. Ceram. Soc. 37 (2017) 3649–3672.
[2] D. Marinha, M. Belmonte, Mixed-ionic and electronic conduction and stability of YSZ-graphene composites, J. Eur. Ceram. Soc. 39 (2019) 389–395.
[3] O.Y. Kurapova, A.G. Glukharev, O.V. Glumov, M.Y. Kurapov, E.V. Boltynjuk, V.G. Konakov, Structure and electrical properties of YSZ-rGO composites and YSZ ceramics, obtained from composite powder, Electrochimica Acta 320 (2019) 134573, https://doi.org/10.1016/j.electacta.2019.134573.
[4] W.Z. Zhu, S.C. Deevi, Development of interconnect materials for solid oxide fuel cells, Mater. Sci. Eng. A 348 (2003) 227–243.
[5] K.W. Schlichting, N.P. Padture, P.G. Klemens, Thermal conductivity of dense and porous yttria-stabilized zirconia, J. Mater. Sci. 36 (2001) 3003–3010.
[6] N. Mahato, A. Banerjee, A. Gupta, S. Omar, K. Balani, Progress in material selection for solid oxide fuel cell technology: a review, Prog. Mater. Sci. 72 (2015) 141–337.
[7] W.J. Quadakkers, J. Piron-Abellan, V. Shemet, L. Singheiser, Metallic interconnectors for solid oxide fuel cells–a review, Mater. High Temp. 20 (2003) 115–127.
[8] N.H. Kwon, G.H. Kim, H.S. Song, H.L. Lee, Synthesis and properties of cubic zirconia–alumina composite by mechanical alloying, Mater. Sci. Eng. A 299 (2001) 185–194.
[9] C. Ramírez, M.I. Osendi, Toughening in ceramics containing graphene fillers, Ceram. Int. 40 (2014) 11187–11192.
[10] C. Ramírez, Q. Wang, M. Belmonte, P. Miranzo, M.I. Osendi, B.W. Sheldon, N.P. Padture, Direct in situ observation of toughening mechanisms in nano-composites of silicon nitride and reduced graphene-oxide, Scripta Mater. 149 (2018) 40–43.
[11] A. Centeno, V.G. Rocha, B. Alonso, A. Fernández, C.F. Gutierrez-Gonzalez, R. Torrecillas, A. Zurutuza, Graphene for tough and electroconductive alumina ceramics, J. Eur. Ceram. Soc. 33 (2013) 3201–3210.
[12] O.T. Picot, V.G. Rocha, C. Ferraro, N. Ni, E. D'elia, S. Meille, et al., Using graphene networks to build bioinspired self-monitoring ceramics, Nat. Commun. 8 (2017) 14425.
[13] H.D. Carlton, J.W. Elmer, D.C. Freeman, R.D. Schaeffer, O. Derkach, G.F. Gallegos, Laser notching ceramics for reliable fracture toughness testing, J. Eur. Ceram. Soc. 36 (2016) 227–234.
[14] M. Turon-Vinas, M. Anglada, Fracture toughness of zirconia from a shallow notch produced by ultra-short pulsed laser ablation, J. Eur. Ceram. Soc. 34 (2014) 3865–3870.
[15] C. Ramirez, P. Miranzo, M. Belmonte, M.I. Osendi, P. Poza, S.M. Vega-Diaz, M. Terrones, Extraordinary toughening enhancement and flexural strength in Si_3N_4 composites using graphene sheets, J. Eur. Ceram. Soc. 34 (2014) 161–169.
[16] M. Belmonte, A. Nistal, P. Boutbien, B. Román-Manso, M.I. Osendi, P. Miranzo, Toughened and strengthened silicon carbide ceramics by adding graphene-based fillers, Scripta Mater. 113 (2016) 127–130.
[17] D. Munz, T. Fett, 'Ceramics: Mechanical Properties, Failure Behavior, Materials Selection', Springer, 1999, p. 300 ISBN 3-540-65376-7.
[18] A. Roine, Outokumpu HSC Chemistry for Windows, V 5.1 (2002).
[19] H. Seiner, C. Ramirez, M. Koller, P. Sedlák, M. Landa, P. Miranzo, et al., Elastic properties of silicon nitride ceramics reinforced with graphene nanofillers, Mater. Design 87 (2015) 675–680.
[20] H.O. Pierson, Handbook of Carbon, Graphite, Diamonds and Fullerenes: Processing, Properties and Applications, William Andrew, 2012.
[21] S.K. Georgantzinos, G.I. Giannopoulos, N.K. Anifantis, Numerical investigation of elastic mechanical properties of graphene structures, Mater. Design 31 (2010) 4646–4654.
[22] G. Tang, Y.L. Shen, D.R.P. Singh, N. Chawla, Analysis of indentation-derived effective elastic modulus of metal-ceramic multilayers, Int. J. Mech. Mater. Des. 4 (2008) 391–398.
[23] M. Belmonte, P. Miranzo, M.I. Osendi, Contact damage resistant SiC/graphene nanofiller composites, J. Eur. Ceram. Soc. 38 (2018) 41–45.
[24] B. Lawn, Fracture of Brittle Solids, Cambridge University Press, 1993, pp. 238–239.
[25] J. Chevalier, C. Olagnon, G. Fantozzi, Crack propagation and fatigue in zirconia-based composites, Compos. Part A Appl. Sci. Manuf. 30 (1999) 525–530.
[26] Z. Li, R.C. Bradt, Micromechanical stresses in SiC-reinforced Al_2O_3 composites, J. Am. Ceram. Soc. 72 (1989) 70–77.
[27] R.W. Steinbrech, Toughening mechanisms in ceramic materials, J. Eur. Ceram. Soc. 10 (1992) 131–142.
[28] Y. Liu, C. Ramirez, L. Zhang, W. Wu, N.P. Padture, In situ direct observation of toughening in isotropic nanocomposites of alumina ceramic, multiwall carbon

nanotubes, Acta Mater. (2017) 203–210.
[29] R.W. Steinbrech, R-curve behavior of ceramics, in: R.C. Bradt, D.P.H. Hasselman, D. Munz, M. Sakai, V.Y. Shevchenko (Eds.), Fracture Mechanics of Ceramics (Composites, R-Curve Behavior, and Fatigue), vol 9, Springer, Boston, 1992.
[30] A. Mukhopadhyay, B.T. Chu, M.L. Green, R.I. Todd, Understanding the mechanical reinforcement of uniformly dispersed multiwalled carbon nanotubes in alumino-borosilicate glass ceramic, Acta Mater. 58 (2010) 2685–2697.
[31] C. Gómez-Navarro, M. Burghard, K. Kern, Elastic properties of chemically derived single graphene sheets, Nano Lett. 8 (2008) 2045–2049.
[32] I. Firkowska, A. Boden, B. Boerner, S. Reich, The origin of high thermal conductivity and ultralow thermal expansion in copper–graphite composites, Nano Lett. 15 (2015) 4745–4751.
[33] K. Chu, X.H. Wang, Y.B. Li, D.J. Huang, Z.R. Geng, X.L. Zhao, et al., Thermal properties of graphene/metal composites with aligned graphene, Mater. Design 140 (2018) 85–94.
[34] P.G. Klemens, Thermal conductivity and lattice vibrational modes, in: F. Seitz, D. Turnbull (Eds.), Solid State Physics, vol. 7, Academic Press, New York, 1958, pp. 1–98.
[35] B. Román-Manso, Y. Chevillotte, M.I. Osendi, M. Belmonte, P. Miranzo, Thermal conductivity of silicon carbide composites with highly oriented graphene nano-platelets, J. Eur. Ceram. Soc. 36 (2016) 3987–3993.
[36] Y. Fan, L. Kang, W. Zhou, W. Jiang, L. Wang, A. Kawasaki, Control of doping by matrix in few-layer graphene/metal oxide composites with highly enhanced electrical conductivity, Carbon 81 (2015) 83–90.